Purine Nucleoside Phosphorylase. 2. Catalytic Mechanism[†]

Mark D. Erion,*[,‡] Johanna D. Stoeckler,[§] Wayne C. Guida,[||] Richard L. Walter,[⊥] and Steven E. Ealick[⊥]

Central Research Laboratory, Ciba-Geigy Ltd., Basel, Switzerland CH4002, Molecular and Biochemical Pharmacology, Brown University, Providence, Rhode Island 02912, Pharmaceuticals Division, Ciba-Geigy Corp., Summit, New Jersey 07901, and Department of Biochemistry, Molecular and Cell Biology, Cornell University, Ithaca, New York, 14853

Received August 7, 1996; Revised Manuscript Received June 30, 1997[⊗]

ABSTRACT: X-ray crystallography, molecular modeling, and site-directed mutagenesis were used to delineate the catalytic mechanism of purine nucleoside phosphorylase (PNP). PNP catalyzes the reversible phosphorolysis of purine nucleosides to the corresponding purine base and ribose 1-phosphate using a substrate-assisted catalytic mechanism. The proposed transition state (TS) features an oxocarbenium ion that is stabilized by the cosubstrate phosphate dianion which itself functions as part of a catalytic triad (Glu89-His86-PO_4═). Participation of phosphate in the TS accounts for the poor hydrolytic activity of PNP and is likely to be the mechanistic feature that differentiates phosphorylases from glycosidases. The proposed PNP TS also entails a hydrogen bond between N7 and a highly conserved Asn. Hydrogen bond donation to N7 in the TS stabilizes the negative charge that accumulates on the purine ring during glycosidic bond cleavage. Kinetic studies using N7-modified analogs provided additional support for the hydrogen bond. Crystallographic studies of 13 human PNP−ligand complexes indicated that PNP uses a ligand-induced conformational change to position Asn243 and other key residues in the active site for catalysis. These studies also indicated that purine nucleosides bind to PNP with a nonstandard glycosidic torsion angle (+*anticlinal*) and an uncommon sugar pucker (C4′-*endo*). Single point energy calculations predicted the binding conformation to enhance phosphorolysis through ligand strain. Structural data also suggested that purine binding precedes ribose 1-phosphate binding in the synthetic direction whereas the order of substrate binding was less clear for phosphorolysis. Conservation of the catalytically important residues across nucleoside phosphorylases with specificity for 6-oxopurine nucleosides provided further support for the proposed catalytic mechanism.

Purine nucleoside phosphorylase (PNP, EC 2.4.2.1)[1] catalyzes the reversible phosphorolysis of purine nucleosides to generate the corresponding purine base and ribose 1-phosphate (Scheme 1). Studies characterizing the reaction by enzyme kinetics indicated that catalysis requires formation of a ternary complex of enzyme, nucleoside, and orthophosphate (Krenitsky, 1967) and that the reaction proceeded without the involvement of phosphorylated or ribosylated enzyme intermediates (Kim et al., 1968). Kinetic data, however, have not consistently supported the same kinetic mechanism nor shown agreement on the order of substrate binding and product release. For example, a Theorell−Chance mechanism has been reported occasionally (Lewis & Lowy, 1979), but most often an ordered bi-bi mechanism is implicated by the kinetic data. In bovine thyroid PNP, phosphate is reported to bind prior to the nucleoside (Carlson & Fischer, 1979), whereas the reverse order is found for bovine brain PNP (Lewis & Glantz, 1976). A study using fluorescence changes to monitor ligand binding concluded that bovine spleen PNP catalyzed phosphorolysis of nucleosides by an ordered bi-bi mechanism with phosphate binding first, whereas nucleoside synthesis proceeded by a random mechanism (Porter, 1992). In contrast, recent studies of PNP-catalyzed hydrolysis (Kline & Schramm, 1992, 1995) and arsenolysis (Kline & Schramm, 1993) of purine nucleosides supported a random substrate binding order in the phosphorolysis direction. One reason for the poor agreement across these studies is likely related to the failure of PNP to obey simple Michaelis−Menten kinetics over a wide range of substrate concentrations and, therefore, the high dependence of the conclusions on the experimental conditions (Parks & Agarwal, 1972; Ropp & Traut, 1991).

The catalytic mechanism of PNP has also been extensively studied by enzyme kinetics. PNP is specific for purine nucleosides in the β-configuration and cleaves the glycosidic bond with inversion of configuration to produce α-ribose 1-phosphate. Bond cleavage is postulated to proceed by an S_N1-type mechanism based on the 20−30% α-deuterium kinetic isotope effect observed during both phosphorolysis (Stein & Cordes, 1981; Lehikoinen et al., 1989) and arsenolysis (Kline & Schramm, 1993) of 1′-[^{2}H]inosine. These results imply that bond breaking is far ahead of bond making in the phosphorolytic direction and that the transition state has considerable oxocarbenium ion character. Further evidence for a transition state with oxocarbenium ion character and weak participation by the nucleophile is apparent from kinetic isotope studies on the PNP-catalyzed

[†] This work was supported by the National Institutes of Health to SEE (P01GM48874, P41RR01646, and CA67763) and by an American Cancer Society grant to JDS (CH-7). SEE is indebted to the W. M. Keck Foundation and the Lucille P. Markey charitable trust.

* Corresponding author: Gensia, Inc., 9360 Towne Centre Drive, San Diego, CA 92121. Telephone: (619) 622-4116. Fax: (619) 622-5545. E-mail: mark.erion@gensia.com.

[‡] Ciba-Geigy Ltd.

[§] Brown University.

[||] Ciba-Geigy Corp.

[⊥] Cornell University.

[⊗] Abstract published in *Advance ACS Abstracts,* September 1, 1997.

[1] Abbreviations: PNP, purine nucleoside phosphorylase; HEPES, *N*-(2-hydroxyethyl)piperazine-*N*′-2-ethanesulfonic acid; R1P, ribose 1-phosphate; TS, transition state; Ino, inosine; Hx, hypoxanthine.

S0006-2960(96)01970-8 CCC: $14.00

Scheme 1

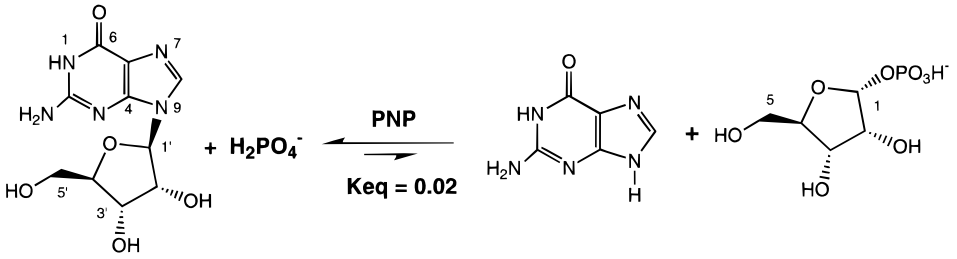

hydrolysis and methanolysis of inosine (Kline & Schramm, 1995). Kinetic studies have also provided some insight into the identity of the active-site residues that participate in catalysis. Log V_{max} vs pH profiles indicated apparent pK_a values of 5.3 and 7.7 (Jordan & Wu, 1978). The lower pK_a value was attributed to either protonation of an active-site histidine (Lewis & Glantz, 1976) or a change in the ionic state of phosphate, i.e., conversion from the active dianion species to the monoanion (Jordan & Wu, 1978). The latter hypothesis is consistent with the finding that the more acidic arsenate is associated with a lower apparent pK_a. The same authors also showed that chemical modification of an active-site histidine by dye-sensitized photooxidation produced a pH-dependent inactivation profile with an apparent pK_a of 6.5. Jordan and Wu concluded from these studies that the more nucleophilic phosphate dianion was the active species and that an active-site histidine might be involved in its deprotonation. Other chemical modification experiments predicted the presence of an active-site arginine, lysine, and cysteine (Salamone & Jordan, 1982; Agarwal & Parks, 1971).

Additional insight into the mechanism of PNP was gained from analysis of the X-ray crystal structure of human PNP (Ealick et al., 1990). The structure indicated that PNP is a homotrimer with each subunit consisting of a distorted β-barrel structure flanked by seven α-helices. The active site is located near the subunit−subunit boundary with seven different segments of one subunit and one segment of the other subunit contributing active-site residues. Three of the four residues predicted by chemical modification experiments were present in the active site, namely His86, Arg84, and Lys244. The critical cysteine, on the other hand, was deduced to be Cys31 based on its position near the entrance of the active site and the likelihood that chemical modification of Cys31 would impede catalysis by sterically blocking substrate entry.

The structure of PNP complexed with both sulfate and psuedosubstrates resistant to phosphorolysis showed the sulfate molecule to reside on the α-face of the nucleoside with one oxygen in position for an in-line attack at C1′. The structure also revealed the active-site residues that were in contact with the PNP substrates, thereby providing some insight into the interactions that were responsible for substrate binding and specificity. Less clear from the X-ray structure were the residues that participate in catalysis. Since each contact with the substrates was through side-chain atoms, a site-directed mutagenesis strategy was employed to help identify the catalytically important residues (Erion et al., 1997). In the study reported herein, we have used site-directed mutagenesis, X-ray crystallography, computer-assisted molecular modeling, protein sequence data, and enzyme kinetics to elucidate the catalytic mechanism. As detailed in the paper following this one, these findings aided our discovery of PNP mutants with novel substrate specificities and catalytic properties useful for the efficient synthesis of nucleosides (Stoeckler et al., 1997).

MATERIALS AND METHODS

Materials. Purine nucleoside phosphorylase from human erythrocytes was purchased as a crude lyophilized powder from Sigma. Xanthine oxidase from buttermilk was obtained from Fluka as a 60% saturated ammonium sulfate suspension. D-Ribose 1-phosphate (estimated purity of 90%), hypoxanthine, guanine, adenine, inosine, guanosine, adenosine, 7-methylguanine, 7-methylguanosine, formycin B, allopurinol, allopurinol riboside, and 2,6-diaminopurine were purchased from Sigma. 9-Deazainosine and 7-deazainosine were gifts from Robert Kline (Montfiore Medical Center).

X-ray Crystallography. Human erythrocytic PNP was obtained as a lyophilized powder and purified as previously described prior to crystallization (Stoeckler, 1984; Ealick et al., 1990). The material was diluted to a final concentration of 14.7 mg/mL in phosphate buffer (pH 7.0) and crystallized by hanging drop vapor diffusion as described previously (Ealick et al., 1990; Cook et al., 1981). Crystal properties were identical to those reported earlier (Ealick et al., 1990): space group $R32$ with hexagonal cell parameters $a = b =$ 142.9 Å, $c =$ 165.3 Å, $a = b =$ 90°, $\gamma =$ 120°. PNP complexes were prepared for data collection by transfer of crystals to a stabilizing mother liquor consisting of 60% saturated ammonium sulfate, pH 5.4. Inhibitor and substrate complex soaks were prepared by dissolving compounds in the artificial mother liquor (2−4 mg/mL), and equilibrating the crystals for approximately 24 h in these solutions prior to data collection.

X-ray intensity data for PNP−ligand complexes were collected using either a Nicolet X-100A detector or a Xuong−Hamlin style twin detector system (San Diego Multiwire Systems, San Diego, CA). Monochromatic CuKα X-rays (1.541 84 Å) were provided by Rigaku RU-200 series rotating anode generators (Rigaku U.S.A., Danvers, MA) operating at 100 mA and 40 kV in both cases. Crystals with dimensions of 0.4−0.5 mm were mounted in glass capillaries for room temperature data collection. For the Nicolet detector, data were collected in 0.25° frames for 3−5 min and were indexed and integrated using the XENGEN data processing programs (Howard et al., 1987). For the Xuong−Hamlin detector, data were collected using ω-scans consisting of 0.1° steps for 30−60 s and were indexed and integrated using San Diego Multiwire Systems software. Final statistics for relevant data are listed in Table 1.

Fractional changes in intensities after relative Wilson scaling were in the range 9−20% when compared to native

Table 1: X-ray Data Statistics for PNP−Ligand Complexes

data set	resolution (Å)	reflections measured	unique reflections	completeness (%)	R_{sym} (%)[a]
guanine[b,d]	3.3	30 825	6895	69	11.2
guanine[b,e]	3.2	36 835	10 484	96	11.1
hypoxanthine[b,f]	3.0	44 514	12 546	95	8.9
hypoxanthine[b,g]	3.0	40 278	10 880	83	9.9
9-deazainosine[c]	3.0	61 249	13 140	100	12.3
7-deazainosine[c]	3.0	58 988	13 131	100	12.9
adenine[c]	3.0	73 058	13 127	100	12.2
adenosine[b]	3.0	62 501	12 481	95	9.3
7-methylguanine[b,h]	3.0	40 488	11 610	88	10.3
allopurinol[c]	3.0	35 475	10 654	81	9.4
allopurinol riboside[c]	3.0	32 243	10 406	79	10.8
Formycin A[c]	3.0	35 288	10 607	81	11.7
2,6-diaminopurine	3.0	24 193	11 112	86	8.6

[a] $R_{sym} = \sum\langle 1\rangle - \mathrm{II}/\sum\langle 1\rangle$. [b] Data sets collected on a Xuong−Hamlin style twin detector system. [c] Data sets collected on a Nicolet X-100A. [d] Prepared as guanosine. [e] Prepared as 2′-deoxyguanosine. [f] Prepared as 2′-deoxyinosine. [g] Prepared as 2′,3′-dideoxyinosine. [h] Prepared as 7-methylguanosine.

data. The largest changes corresponded to complexes involving a substrate-induced conformational change. Difference Fourier maps for complexes were calculated using all data between 15 Å and the highest available resolution, typically 2.8−3.1 Å, $|F_{O(complex)} - F_{O(native)}|$ as coefficients, calculated phases (native) between 5 and 2.8 Å, and multiple-isomorphous-replacement phases between 15 and 5 Å. Ligands were visible as the largest peaks in the electron density maps with peak heights ranging from approximately 10.0−16.0 times the root mean square background of the map. In all cases the ligand binding site was consistent with the previously published nucleoside binding site for PNP (Ealick et al., 1990).

Difference electron density maps were displayed on a Silicon Graphics VGX 4D/440 workstation using the interactive graphics program CHAIN (Sack, 1988). The previously refined model of native PNP (Ealick, 1990; Symersky, unpublished results) was used as a source of initial protein coordinates. The program MacroModel (Mohamadi et al., 1990) was used to generate coordinates for the structures of ligands which were subsequently fit to the experimental electron density. Similarly, conformational changes in the protein were modeled by refitting native residues into peaks in the electron density. After manual fitting, the coordinates were prepared for refinement in the XPLOR package (Brünger, 1992). Complex structures were refined by cycles of simulated annealing and conjugate gradient minimization with an initial temperature of 4000 K and a timestep of 0.25 ps. Unmodified XPLOR topology and parameter files were used for the protein structure while those for nucleoside ligands were modified from toph11.dna and param11.dna. Refinement cycles were alternated with manual refitting using $2F_O - F_C$ and $F_O - F_C$ maps until no further changes occurred in the model. The final model had root mean square deviations from ideality ranging from 0.012 to 0.020 Å for bond distances and 1.5 to 2.0° for bond angles. Final *R* factors for refined complex structures ranged from 17 to 22%.

Steady-State Substrate Kinetics. Kinetic parameters for 7-methylguanosine and 7-methylguanine with wild-type and the two Asn243 mutants, Asn243Ala (Erion et al., 1997) and Asn243Asp (Stoeckler et al., 1997), were determined spectrophotometrically from the change in absorbance at 260 nm

Scheme 2

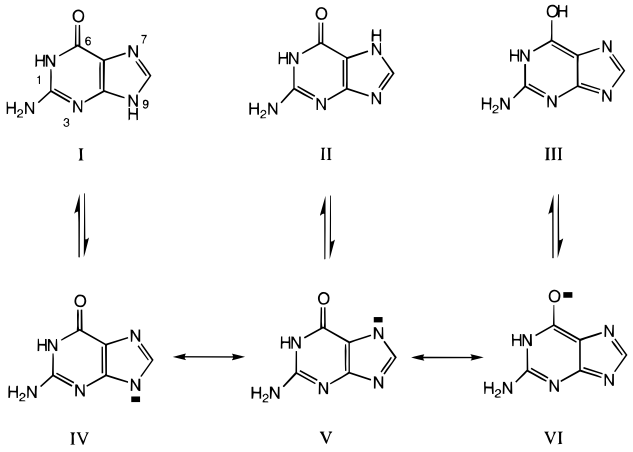

(Bzowska et al., 1990). Reactions were conducted in 100 mM HEPES, pH 7, at 30 °C containing either 50 mM phosphate or 10 mM R1P as the second substrate. 7-Methylguanosine was synthesized by incubating 880 μM 7-methylguanine with 10 mM ribose 1-phosphate and 60 μg of wild-type PNP in 100 mM HEPES buffer, pH 7, for 10 min at 25 °C. To confirm the product structure, the sample was deproteinated by centrifugal ultrafiltration and analyzed on a Varian 5000 Liquid Chromatograph. A Waters μBondapak C_{18} column was eluted at 1 mL/min with 1 mM potassium phosphate, pH 7, employing a linear gradient of 0 to 50% (from 1−11 min) methanol. 7-Methylguanine and its corresponding nucleoside emerged at approximately 8 and 10 min, respectively. Both compounds were monitored at 282 nm with a Kratos Spectroflow 757 absorbance detector. Elution of 7-methylguanosine was also monitored with a Kratos Spectroflow 980 fluorescence detector, $\lambda_{exc} = 270$ nm (Kulikowska et al., 1986). Conversion of the nonfluorescent base to the fluorescent nucleoside (approximately 20% under these conditions) required the presence of both enzyme and ribose 1-phosphate. The fluorescent product peak was eliminated by further addition of PNP and 100 mM phosphate to reverse the reaction. Synthesis of allopurinol riboside catalyzed by wild-type and mutant PNP was monitored by HPLC as described above, except that peaks were eluted with water and monitored at 251 nm. Incubations were carried out at 30 °C for 30, 60 or 120 min. The 200 μL reaction volumes contained 10 mM ribose 1-phosphate, 0.1 M HEPES, pH 7, and either 0.163 μg of wild-type, 32.9 μg of Asn243Ala, or 13.7 μg of Asn243Asp PNP. Retention times for allopurinol and allopurinol nucleoside were approximately 10.2 and 12.5 min, respectively.

Energy Calculations: *Guanine Tautomers.* Relative electronic energies of the N9, N7, and O6 tautomers of guanine (Scheme 2) were computed using ab initio molecular orbital calculations at the Hartree−Fock (HF) level. The Gaussian 92/DFT program running on an IBM RS 6000/590 was used for these calculations (Revision 6.4, Frisch et al., 1993). Each structure was built and then subjected to molecular mechanics-based energy minimization with the AMBER* force field using the MacroModel/BatchMin software (version 3.5) (Mohamadi et al., 1990). The structures were then imported into Gaussian and each structure was subjected to further geometry optimization using the HF molecular orbital method at the 6-31G** level. These calculations were followed by a single point energy calculation at the MP2/6-31G** level.

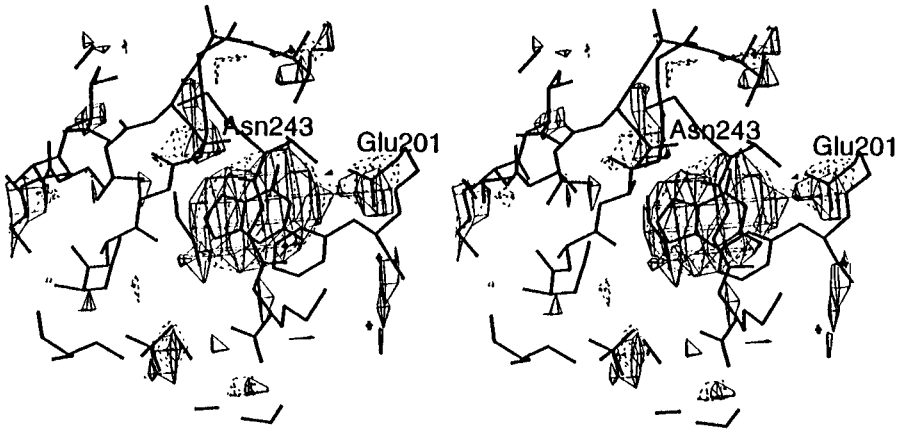

FIGURE 1: Difference electron density for representative PNP−ligand complexes. Side-by-side stereoview of difference electron density maps showing density for the bound substrate base, hypoxanthine, and protein conformational changes at Asn243 and Glu201. The superimposed maps were calculated from data collected on PNP crystals equilibrated with the nucleosides inosine (solid lines) and 2′-deoxyinosine (dashed lines).

In addition, hydration energies for the N9 and N7 tautomers were estimated using the GB/SA continuum solvation model available in BatchMin. Charges used in the calculation were obtained by fitting the charges to the electrostatic potential, which was derived from the MP2/6-31G** calculations.

Nucleoside Conformation. The relative energy of inosine in the X-ray conformation vs the standard *anti* conformation was computed using the SPARTAN software (version 3.1, Wavefunction, Inc., Irvine, CA) running on the Silicon Graphics 4D/480. The high *anti* (*-synclinal*) conformation of inosine (O−C1′−N9−C4 torsion angle = −60°, sugar pucker = C3′ *endo*) was built using the MacroModel/BatchMin software and subjected to energy minimization using the united atom AMBER* force field. The structure was then imported into SPARTAN and subjected to further geometry optimization using the ab initio HF molecular orbital method at the 3-21G(*) level. The X-ray derived conformation of inosine was obtained by adjusting the O−C1′−N9−C4 torsion angle of the 3-21G(*) optimized high *anti* conformer. A value of 133° was selected based on the angle observed in the X-ray structure of the PNP−9-deazainosine complex. Geometry optimization with SPARTAN at the HF 3-21G(*) level was carried out with the O−C1′−N9−C4 torsion angle constrained to maintain a value of 133°. Each conformer was then subjected to a single point energy calculation at the HF/6-21G** level.

RESULTS

Structures of PNP−Ligand Complexes. X-ray crystallographic data were measured for 13 complexes of PNP and various substrate analogs (Table 1). In most cases, the data were measured to 3.0 Å resolution with data completeness ranging from 69 to 100%. Although the R_{sym} values were somewhat high (8.9−12.9%), the redundancy of measurement was 3−5 observations per unique reflection and the electron density maps were unambiguous (Figure 1).

Structure of PNP−6-Oxopurine Complexes. Crystals of PNP treated with either guanosine or 2′-deoxyguanosine showed only the purine base apparently as a result of PNP-catalyzed nucleoside hydrolysis in the crystal. Likewise, crystals treated with 2′-deoxyinosine or 2′,3′-dideoxyinosine showed only density for hypoxanthine. The resulting guanine and hypoxanthine complexes showed additional positive density around the side chain of Asn243 and Glu201, indicating that these two side chains were more ordered in the complex then in the unliganded structure. The guanine and hypoxanthine complexes showed similar binding interactions and active-site structures. The side chain of Asn243 forms a hydrogen bond with N7 and possibly O6 of the purine while Glu201 accepts a hydrogen bond from N1. The conformational change previously reported (Ealick et al., 1990) for residues 241−265 was observed in complexes for all 6-oxopurine analogs and is illustrated in Figure 2. The conformational change results in an extension at the N-terminal end of the C-terminal helix by about eight residues (257−264) and displaces His257 away from the active-site cavity. Lys244 is also extended away from the active site and does not interact with the purine base. Crystals treated with 7-methylguanosine yielded the 7-methylguanine complex. The binding of 7-methylguanine was similar to that of guanine and hypoxanthine.

Structure of PNP−6-Oxopurine Nucleoside Complexes. Crystals of PNP treated with noncleavable analogs 9-deazainosine or 7-deazainosine provided details of the nucleoside conformation and binding. Each nucleoside analog differed at N7, since the N7 position in 9-deazainosine acts as a hydrogen bond donor whereas N7 in inosine is a hydrogen bond acceptor and the CH in both 7-deazainosine and allopurinol riboside eliminates the possibility of a hydrogen bond at this position. Despite these differences, all three analogs exhibited the same overall purine binding orientation and position in the active site. The ribosyl group of the nucleoside analogs formed hydrogen bonds between O3′ and Tyr88 and between O5′ and His257. The hydrophobic face of the ribosyl group interacted with the side chain of Met219 and was pointed away from the phosphate binding site. The glycosidic bond was in the +*ac* conformation and the sugar pucker was near the C4′-*endo* conformation. This geometry orients the nucleoside so that C1′ is near an oxygen of the phosphate ion.

Structure of PNP−6-Aminopurine Complexes. Crystals treated with adenine or allopurinol showed that the locations of 6-oxopurines and 6-aminopurines in the active site are similar. Difference electron density maps exhibited clear density for the 6-aminopurine; however, the conformational change observed for residues 241−265 in the 6-oxopurine complexes was absent. The adenine molecule was accom-

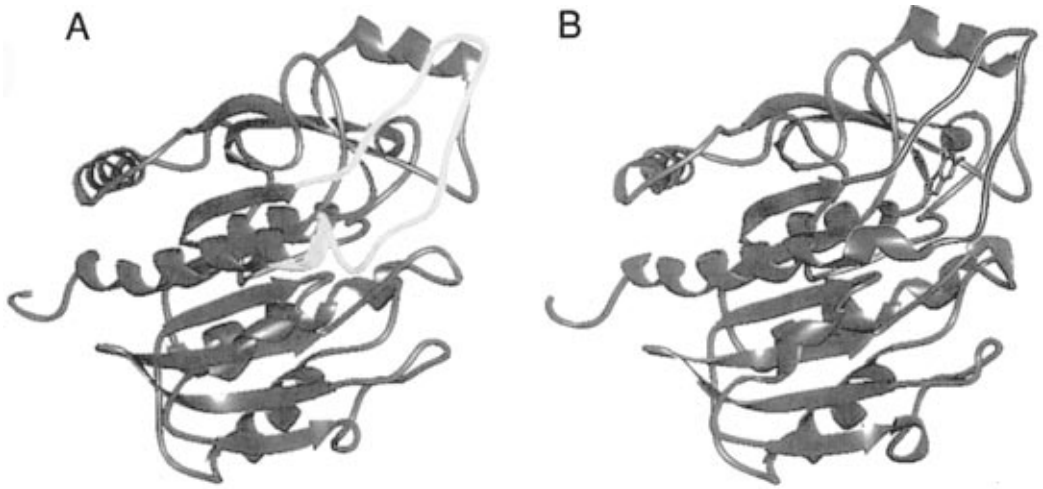

FIGURE 2: Ligand-induced conformational change in PNP. Ribbon schematics of the refined structures of (A) native PNP and (B) a guanine complex of PNP. The highlighted regions (yellow for native and red for complex) are residues 240−265, which undergo a structural disorder to order transition upon substrate binding. Guanine is also represented in the purine binding site and colored accordingly (red) for the complex. Panel A shows residues 257−265 as a disordered loop whereas panel B shows these residues as a 1.5 turn extension of the C-terminal helix. Figure generated using the program RIBBONS (Carson & Bugg, 1986).

FIGURE 3: Binding conformation of purine nucleosides in the PNP active site. Side-by-side stereoview overlap showing the agreement in binding position and conformation of four noncleavable substrate analogs. The compounds were each soaked into crystals of PNP and the three-dimensional structures were determined and refined independently. The nucleosides are 7-deazainosine (blue), 9-deazainosine (red), allopurinol riboside (green), and formycin A (magenta). Figure generated using the program RIBBONS (Carson & Bugg, 1986).

modated in the active site with only slight readjustment of side chains, and no significant electron density was observed beyond the base itself.

Structure of PNP−6-Aminopurine Nucleoside Complexes. Crystals of PNP treated with adenosine or Formycin A showed density for both the base and the ribosyl group. The presence of the ribosyl group suggested that these compounds were poor PNP substrates, since 6-oxopurine nucleosides, which are known to undergo phosphorolysis in the presence of PNP, showed density for only the base. The overall binding of the 6-aminopurine nucleosides was similar to that of the 6-oxopurine nucleosides with the glycosidic torsion angle in the +*ac* conformation (Figure 3). As was the case for the 6-aminopurines, no conformational change was observed in residues 240−265.

Pseudosubstrate Kinetic Analyses. Consistent with results previously reported in the literature, allopurinol riboside, like other 7-deazapurine nucleoside analogs, was resistant to phosphorolysis (Krenitsky et al., 1968) whereas allopurinol was a substrate of PNP (Krenitsky et al., 1967). Analysis of allopurinol with wild-type PNP and the Asn243Ala and Asn243Asp mutants showed catalytic efficiencies of 2×10^4 M^{-1} s^{-1} for wild-type PNP and between 20 and 40 M^{-1} s^{-1} for the two mutant PNPs (Table 2). Results shown in Table 2 also indicated that in comparison to guanosine the wild-type enzyme catalyzes the phosphorolysis (Jordan & Wu, 1978; Bzowska et al., 1990) and synthesis of 7-methylguanosine with 1.6-fold higher and 200-fold lower catalytic efficiencies, respectively. Kinetic analyses of the Asn243Ala and Asn243Asp mutants with 7-methylguanosine as substrate revealed an increase in phosphorolysis efficiency relative to wild-type of 3.1- and 2.4-fold, respectively; both mutants also exhibited a 1.8-fold increase in synthesis efficiency. Relative to guanosine, however, the phosphorolytic efficiencies of the Asn243Ala and Asn243Asp mutants with 7-methylguanosine represented a remarkable 11000- and 435-fold increase, respectively. As Table 2 indicates, the large preference for 7-methylguanosine over guanosine by the mutant PNPs is attributed almost exclusively to changes in k_{cat} with the K_M for 7-methylguanosine only decreasing 2- and 6-fold relative to guanosine for the Asn243Ala and Asn243Asp mutants, respectively.

7-Methylguanine is reported to be a weak inhibitor of calf spleen PNP at concentrations 10−20-fold higher than those used for inosine synthesis (Bzowska et al., 1990; Kulikowska et al., 1986). In contrast, 7-methylguanine is a reasonably good substrate for wild-type human PNP as well as the Asn243Ala and Asn243Asp mutants with the k_{cat}s reduced less than 4-fold relative to guanine (Table 2). The ability of hPNP to catalyze the synthesis of 7-methylguanosine was confirmed by HPLC (see Materials and Methods).

Energy Calculations. Relative energies of the N9, N7, and O6 tautomers of guanine were computed using ab initio molecular orbital calculations at the Hartree−Fock and MP2 levels. Results from these gas phase calculations indicated that the N9 (**I**) and N7 (**II**) tautomers (Scheme 2) are close in energy (∼0.5 kcal/mol) while the O6 tautomer (**III**) was over 20 kcal/mol higher in energy. Similarly, the hydration energies were nearly equal for the N7 and N9 tautomers. These results were consistent with studies showing the presence of both the N7(H) and N9(H) tautomers of guanine (Pfleiderer, 1961) and adenine (Dreyfus et al., 1974) in aqueous solutions.

The relative energy difference was calculated for inosine starting with a standard high *anti* glycosidic torsion angle

Table 2: Kinetic Parameters of 7-Modified Purine Nucleoside Analogs with PNP and Asn243 PNP Mutants

	wild-type			Asn243Ala[a]			Asn243Asp[b]		
substrate	K_M (μM)	k_{cat} (s^{-1})	k_{cat}/K_M[d] (s^{-1} M^{-1})	K_M (μM)	k_{cat} (s^{-1})	k_{cat}/K_M[d] (s^{-1} M^{-1})	K_M (μM)	k_{cat} (s^{-1})	k_{cat}/K_M[d] (s^{-1} M^{-1})
guanosine[b]	12 ± 1	26 ± 2	2.3	42 ± 1	0.050 ± 0.001	0.001	140 ± 20	2.8 ± 0.4	0.02
guanine[b]	6 ± 0.7	48 ± 1	8	120 ± 17	26 ± 1	0.21	50 ± 5	29 ± 1	0.58
7-methylguanosine	14.3 ± 0.3	50 ± 10	3.6	17 ± 2.5	190 ± 12	11	22 ± 2	190 ± 27	8.7
7-methylguanine	290 ± 38	11 ± 0.4	0.04	190 ± 40	13 ± 0.3	0.07	220 ± 8	15 ± 2	0.07
allopurinol	86 ± 5	2.1 ± 0.1	0.02	250 ± 14	0.005 ± 0.0002	0.00002	250 ± 42	0.009 ± 0.0005	0.00004
allopurinol riboside		ND[c]			ND[c]				

[a] Erion et al., 1997. [b] Stoeckler et al., 1997. [c] ND: No activity detected. [d] Values have been multiplied by 10^{-6}.

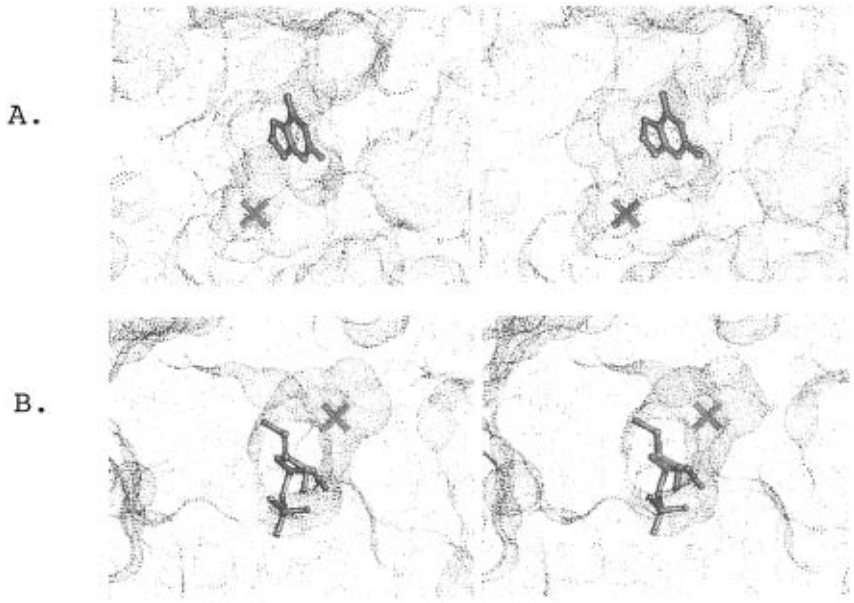

FIGURE 4: Active-site volume map of PNP−substrate complexes. Dot surface representations of the accessible surface in the active site region of PNP for complexes with the substrates (A) hypoxanthine and (B) ribose 1-phosphate (R1P). In panel A, access to the active site is not restricted by the presence of the purine base ligand which is deeply buried. However, panel B shows that the entrance to the active site, and access to the purine binding site, is obstructed by the presence of R1P. Panel A was calculated from the refined structure of human PNP complexed with guanine while panel B was calculated from the bovine enzyme's structure (Mao, C., unpublished results). The bovine structure was used for the latter because of the inability to prepare the R1P complex with the human enzyme due to the high concentration of sulfate in the crystallization buffer and, therefore, the presence of sulfate in the phosphate binding site. The dot surfaces were calculated in RIBBONS (Carson & Bugg, 1986) using a probe radius of 1.6 Å.

(O−C1′−N9−C4) of −60° (Saenger, 1984a) and inosine with a glycosidic torsion angle equal to the torsion angle found in the PNP−9-deazainosine complex (O−C1′−N9−C4 torsion angle = 133°, sugar pucker = C4′ *endo*) and similar to the average torsion angles found for all nucleosides bound to PNP (Figure 3). Geometry optimization of the high *anti* conformation (C3′-*endo* sugar pucker) at the HF 3-21G(*) level afforded a torsion angle of −156°, which is consistent with experimentally derived structures. Geometry optimization of inosine in the binding conformation at the HF 3-21G(*) level led to rapid deviation of the sugar pucker away from the initial C4′ *endo* geometry and to poor convergence. However, constrained geometry optimization using a sugar pucker of C3′ *endo* as described above yielded a minimum energy structure. The energy of this conformer was 3.28 kcal/mol higher in energy than the minimized conformer starting in the high *anti* conformation. Furthermore, the corresponding C4′ *endo* conformer is predicted to have an even greater energy difference based on the higher conformational energy associated with this sugar pucker and the nucleoside binding conformation (Saenger, 1984a).

DISCUSSION

Substrate Binding and Product Release. Steady-state kinetic data for PNPs isolated from a variety of tissues and species have supported several different kinetic mechanisms. Although an ordered bi-bi mechanism is the mechanism most often proposed, no clear agreement has been reached on the nature (random or ordered) and order of substrate binding and product release. PNP−ligand X-ray structures provide an alternative method for ascertaining the order of ligand binding. Analysis of the structure for the PNP−sulfate[2] complex indicated that the active site is in a deep cavity at the interface of two subunits. The purine subsite is located farthest from the solvent interface, whereas the ribosyl subsite is closest. On the basis of a graphical analysis (Figure 4),

[2] Sulfate binds to the phosphate binding site and is present in the human PNP X-ray structures as a result of the high concentration of ammonium sulfate in the crystallization buffer. Sulfate and phosphate are structurally similar based on geometry (tetrahedral), anionic charge (four negatively charged oxygen atoms), and molecular size (similar bond angles and bond distances). Accordingly, references in the text to crystal structures and their support for the catalytic mechanism assume that no large structural perturbations exist between the PNP−sulfate and the PNP−phosphate complexes.

Scheme 3

both the purine base and ribose 1-phosphate subsites appeared readily accessible and the ribose binding site remained accessible even after a purine base was appropriately positioned in the purine binding site. In contrast, the purine subsite appeared to be blocked in the PNP−ribose 1-phosphate complex, which suggested that an initial ribose 1-phosphate binding might result in a dead-end complex. On the other hand, initial purine binding, based on results discussed below, may result in a conformational change that promotes additional interactions between PNP and ribose 1-phosphate and thereby facilitates formation of the ternary complex. Accordingly, these data support ordered binding in the synthetic direction with purine base binding preceding ribose 1-phosphate (Scheme 3, Figure 5).

In the phosphorolysis direction, the order of substrate binding was less clear. Graphical analysis of the PNP−phosphate complex indicates that phosphate partially blocks nucleoside access to the binding site. These results suggest ordered substrate binding in the phosphorolysis direction with the nucleoside binding prior to phosphate (Figure 5). Random substrate binding, however, cannot be completely ruled out on the basis of structure alone since slight adjustments in the active-site structure could enable nucleoside binding to the PNP−phosphate complex.

Ligand-Induced Conformational Change. A comparison of the native PNP structure (Ealick et al., 1990) with PNP−inhibitor (Ealick et al., 1991; Montgomery et al., 1993, Erion et al., 1993) and PNP−substrate analog complexes showed considerable movement of active-site residues upon binding of the ligand. The largest movement was observed for the His257 side chain, which partially occupies the purine subsite in the native enzyme. Upon binding of the purine base, His257 is displaced outward by more than 5 Å. This movement leads to reorganization of a flexible loop of residues (241−265) that makes up part of the active site as well as the subunit−subunit interface. Analysis of 13 PNP−nucleoside and PNP−base complexes showed that the structure of the loop is ligand dependent. The X-ray structures of PNP complexed to 6-oxopurines or the corresponding nucleoside analogs showed that the loop reorganizes to extend the C-terminal helix (Figure 2B) and that the extension results in additional contacts between the purine base and the protein. In contrast, PNP complexed to 6-aminopurines or the corresponding nucleoside analogs showed the loop to remain relatively disordered. Since inosine is a 10^6-fold better substrate than adenosine, the conformational change appears to be associated with catalysis (Zimmerman et al., 1971; Stoeckler et al., 1997). The residues most affected by binding of a catalytically competent substrate include His257, Thr242, Asn243, and Lys244. Of these, only His257 and Asn243 directly interact with the substrate and only Asn243 appears to be important for catalysis based on mutagenesis results (Erion et al., 1997). These data therefore suggest that nucleoside phosphorolysis occurs after the ligand-induced conformational change and

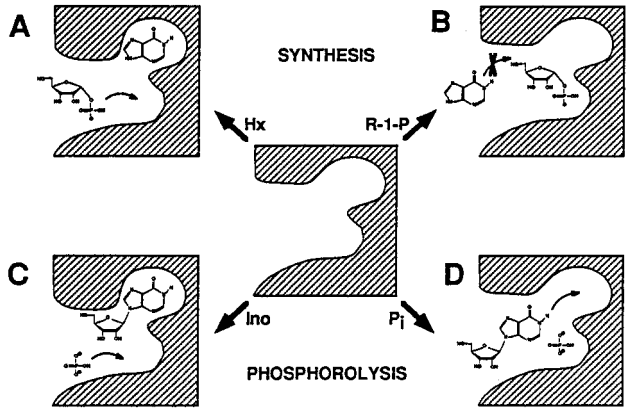

FIGURE 5: Cartoon of substrate binding in the phosphorolytic and synthetic directions. The upper (synthesis) portion of the diagram shows the structural outcome of first binding (A) hypoxanthine resulting in the E·Hx complex or (B) ribose-1-phosphate resulting in the E·R-1-P complex. In the latter case, access to the purine binding site is blocked. The lower (phosphorolysis) portion of the diagram shows the outcome of binding first (C) nucleoside resulting in the E·Ino complex or (D) phosphate resulting in the E·Pi complex. The active site conformational change caused by purine binding is represented as a constriction of the active site opening in panels A and C.

that the conformational change enables catalysis by aiding formation of a hydrogen bond between the purine and Asn243.

Role of the Purine Binding Site in Phosphorolysis. Chemical hydrolysis of purine nucleosides proceeds at low pH by rate-limiting heterolysis of the mono- or diprotonated nucleoside to yield the purine base and an intermediate ribosyl oxocarbenium ion (Romero et al., 1978). The site of protonation is reported to be N7 based on studies of purine nucleoside analogs, including studies which indicate that 7-deazaadenosine and 8-hydroxyadenosine are resistant to acid hydrolysis and that 7-methylguanosine hydrolyzes in a pH-independent manner (Zoltewicz et al., 1970). Protonation of the purine base accelerates the reaction by generating positive charge on the base which in turn enhances the leaving group ability. Strong mineral acids are required to protonate the base since the pK_a of nucleosides such as guanosine is less than 2 (Saenger, 1984).

The mechanistic details of enzyme-catalyzed purine nucleoside hydrolysis are less well-defined. Kinetic studies on AMP nucleosidase indicated that glycosidic bond cleavage occurs by an S_N1-type mechanism (Parkin et al., 1991; Horenstein et al., 1991). Analogous to the mechanism for acid-catalyzed purine nucleoside hydrolysis, an acidic amino acid residue was postulated to reside near N7 and to participate in the catalytic mechanism. Use of an acidic group to enhance glycosidic bond cleavage is well precedented based on the catalytic mechanisms reported for glycosidases. For example, X-ray structures of lysozyme−substrate complexes support a catalytic mechanism that involves protonation of the exocyclic oxygen of the glycosidic bond by Asp52 prior to cleavage of the oligosaccharide (Blake et al., 1967).

Examination of the purine binding site in the X-ray structures of PNP complexed with a variety of purine nucleoside analogs failed to identify an acidic residue in contact with N7. Instead, an acidic residue, namely Glu201, was found near N1 and only the Asn243 side-chain carboxamido group was found in the vicinity of N7. Neverthe-

less, replacement of each residue with alanine resulted in mutant proteins exhibiting catalytic efficiencies ≥1000-fold lower than wild-type (Erion et al., 1997). The reduced phosphorolytic efficiency of the Glu201Ala mutant is primarily a result of a large increase in substrate K_M. The modest effect of this mutation on k_{cat} is not surprising for several reasons. First, the carboxylate of Glu201 appears to exist as the carboxylic anion based on X-ray structures of PNP complexes, which consistently show the carboxylate to be rigidly held in the plane of the purine base and to be in position to simultaneously accept a hydrogen bond from N1 with one oxygen and a hydrogen bond from the 2-amino group of guanine with the other oxygen. As a carboxylic anion, Glu201 is not expected to stabilize the TS, since glycosidic bond cleavage should increase negative charge on the purine base. Second, even if Glu201 exists in the protonated from and is used to protonate N1 of 6-oxypurine nucleosides (enolic form),[3] the catalytic benefit would be questionable.[4] For example, mechanistic studies of adenosine hydrolysis indicate that, although protonation of adenosine initially occurs at N1, glycosidic bond cleavage occurs only after protonation of N7 and generation of the diprotonated species (Garrett & Mehta, 1972; Lonnberg & Lehikoinen, 1982). Other data that makes Glu201 an unlikely participant in the glycosidic bond breaking and bond forming steps is apparent from comparing the sequences for PNP and another mechanistically similar phosphorylase, namely methylthioadenosine phosphorylase (MTAP). In MTAP, Glu201 is replaced with Ser whereas most of the other active-site residues are conserved (Erion et al., unpublished results). These results suggest that the carboxylate of Glu201 is not directly involved in catalysis but rather may assist catalysis through binding of the substrate in a catalytically competent orientation.[5]

In contrast to Glu201, the participation of Asn243 in the catalytic mechanism is supported by a multitude of experimental findings. The importance of Asn243, however, was not readily apparent in the native PNP X-ray structure where the side-chain carboxamido group was originally positioned to donate a hydrogen bond to O6 (Ealick et al., 1990) or in subsequent structures of PNP complexed with 9-deazapurine analogs where the side-chain carbonyl was reoriented relative to the native structure to accept a hydrogen bond from the N7 hydrogen (Ealick et al., 1991). In addition, X-ray structures of PNP complexed with purine nucleoside substrates, e.g., inosine or guanosine, were not available due to the instability of these compounds to the crystal growth conditions. The position and therefore the hydrogen-bonding interactions of Asn243 was therefore largely surmised from active-site modeling studies of PNP with purine analogs. These studies indicated that Asn243 could donate a hydrogen bond to N7. Recent studies using bovine PNP have resulted in high-resolution crystal structures of PNP complexed to purine nucleosides in the absence of phosphate or sulfate. These studies confirmed the modeling studies and indicated that in addition to N7, the carboxamido group donates a hydrogen bond to the Thr242 hydroxyl (Mao, C., & Ealick, S. E., unpublished results).

The importance of Asn243 to catalysis was further suggested by the finding that the Asn243Ala mutant exhibited a 1000-fold decrease in catalytic efficiency relative to wild-type (Erion et al., 1997). The importance of the hydrogen bond between Asn243 and N7 of the purine base is supported by studies of N7-modified purine nucleoside analogs with PNP and with the Asn243Ala mutant. For example, 7-deazapurine nucleosides fail to undergo PNP-catalyzed phosphorolysis presumably because they are unable to accept an analogous hydrogen bond (Stoeckler, 1984). On the other hand, 7-methylguanosine, which is also unable to accept a hydrogen bond at N7 undergoes efficient phosphorolysis in the presence of PNP (Jordon & Wu, 1978; Bzowska et al., 1990). This result suggests that the Asn243 side chain accommodates the N7-methyl group by rotating away from the base and that phosphorolysis proceeds independent of Asn243 because the positive charge at N7 of 7-methylguanosine enhances the leaving group ability of the purine base to a degree similar to the Asn243−N7 hydrogen bond. Accordingly, 7-methylguanosine was a good substrate for the Asn243Ala mutant with a catalytic efficiency approximately 5-fold better than guanosine with wild-type PNP. This catalytic efficiency represents a remarkable 11000-fold improvement in efficiency relative to the Asn243Ala mutant with guanosine, which is attributed primarily to a 4000-fold enhancement in k_{cat}.

Further support for the participation of the Asn243−N7 hydrogen bond in catalysis is revealed by the strict conservation of Asn243 in all phosphorylases with specificity for O6-purine nucleosides (Figure 6). Since only 12% of the residues are completely conserved for all nine sequences, the likelihood that the observed Asn243 conservation is due to chance is low. Other catalytically important residues such as Glu201 are also conserved.

The large catalytic role for Asn243 is consistent with the stabilization expected for a hydrogen bond to a negatively charged N7 in the TS (Figure 7). Hydrogen bonds to charged groups have been reported to be worth 3.5−4.5 kcal/mol (Fersht et al., 1985), which is a value similar to the stabilization expected following full protonation of N7 in acid-catalyzed nucleoside hydrolysis. Use of a hydrogen bond to stabilize a negatively charged TS is analogous to the catalytic mechanisms ascribed to serine and cysteine proteases. In these enzymes, an Asn or a Gln resides in the "oxyanion hole" and stabilizes the TS by using the carboxamido group to donate a hydrogen bond to the negatively charged tetrahedral intermediate that forms following addition of the serine or cysteine to the peptide bond (e.g., Asn155 of subtilisin; Wells et al., 1986).

[3] Spectroscopic studies and theoretical calculations indicate that the 6-keto tautomer is the predominate tautomeric form under normal physiological conditions (>99.99%; Saenger, 1984a). Nevertheless, the enol tautomer cannot be ruled out by these studies, since Glu201 could exist in the protonated form and thereby stabilize the enol tautomer through donation of a hydrogen bond to N1.

[4] One possible benefit of the enolic form could be the formation of a hydrogen bond between the 6-hydroxyl group and the carbonyl of Asn243 which in turn could strengthen the hydrogen bond in the TS between the Asn243 amido hydrogen and N7. Although structurally possible after relatively minor side chain adjustments, this hydrogen bond pattern seems less likely since it would also be predicted for 6-aminopurines and thereby not readily account for the large substrate preference of PNP for 6-oxopurines over 6-aminopurines (Stoeckler et al., 1997).

[5] The hydrogen bond formed between N1 and Glu201 may also assist catalysis by limiting the existence of the N1 monoanion. The monoanion ($pK_a \approx 9$ for hypoxanthine and inosine; Izatt et al., 1971) could slow purine base deprotonation at N9 (second $pK_a \approx 12$) and thereby compromise catalytic efficiency in the nucleoside synthesis direction. Similarly, the monoanion would make the base a worse leaving group thereby decreasing catalytic efficiency in the phosphorolysis direction.

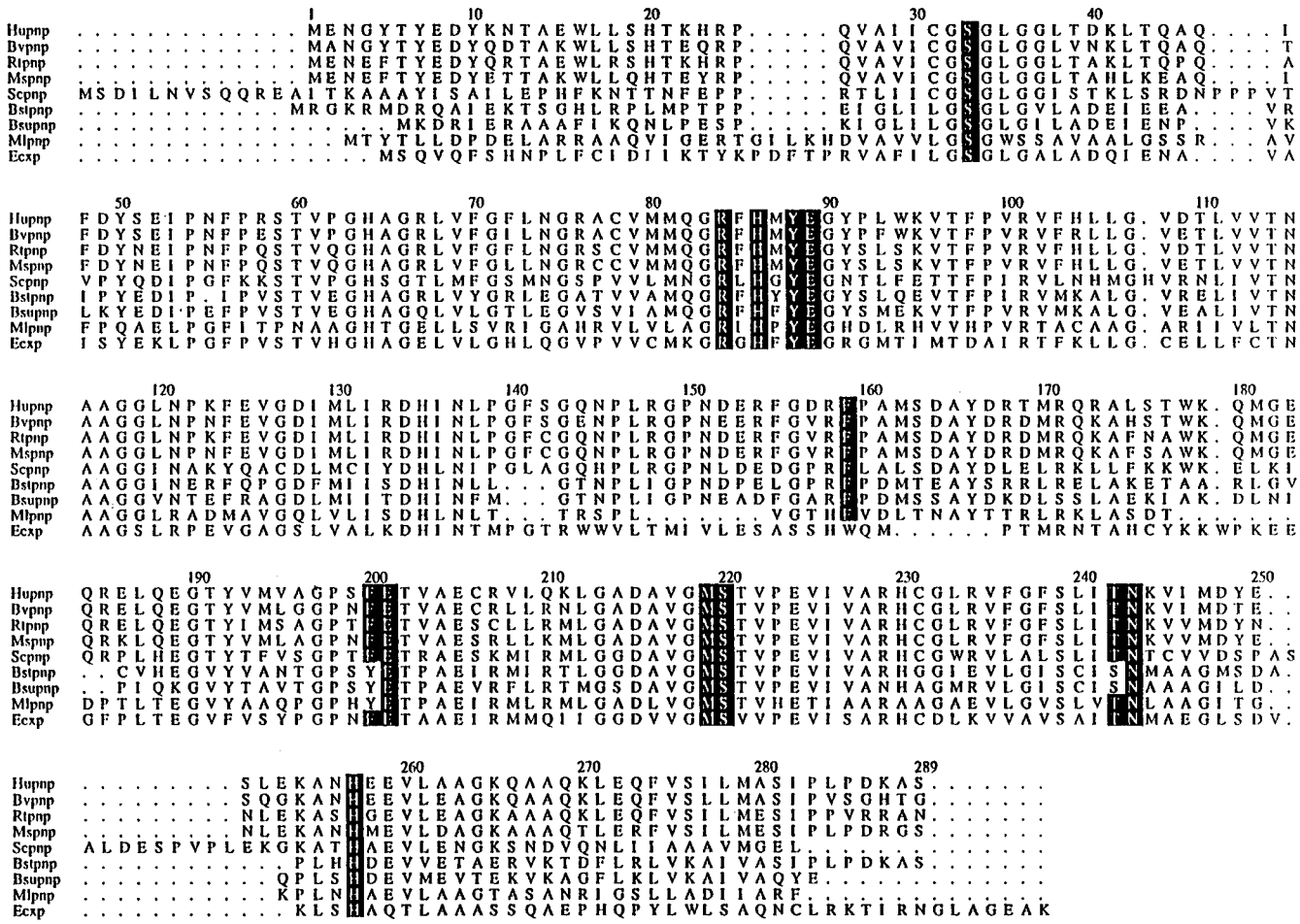

FIGURE 6: Comparison of amino acid sequences of PNPs. Hupnp = human PNP (Williams et al., 1984); BvPNP = bovine PNP (Bzowska et al., 1995); Rtpnp = rat PNP; Mspnp = mouse PNP (Jenuth & Snyder, 1991); Scpnp = *Saccharomyces cerevisiae* PNP (Pauley, A), Bsupnp = *Bacillus stearothermophilus* PNP; Bsupnp = *Bacillus subtilis* PNP (Schuch et al., 1995); Mlpnp = *Mycobacterium leprae* PNP (Robinson, 1993), Ecxp = *Escherichia coli* xanthosine phosphorylase (Seeger et al., 1995).

Role of the Purine Binding Site in Nucleoside Synthesis. In the synthetic direction, the purine base adds to C1′ either with simultaneous displacement of phosphate (S_N2 reaction) or following formation of an intermediate oxocarbenium ion generated after phosphate dissociation (S_N1 reaction). In either case, N9−C1′ bond formation implies that N9 has a pair of electrons available for the reaction. Consequently, for the reaction to proceed, the purine base must exist in the deprotonated form of **I** (i.e., **IV**), as tautomers **II** or **III**, or as their corresponding monoanions **V** or **VI** (Scheme 2).

Graphical analysis of the PNP structure suggested that all three purine base forms are readily accommodated by the purine subsite. Negative charge at N7 or at O6 as found in resonance structures **V** and **VI**, respectively, would be stabilized through hydrogen bond donation by Asn243 to N7 and O6 and through possible protonation of O6 by Glu201 via a bridging water molecule. The N7(H) tautomer, **II**, is accommodated by the purine subsite through a minor movement in the Asn side chain such that the N7 hydrogen forms a hydrogen bond with the Asn243 side-chain carbonyl and O6 maintains a hydrogen bond to one of the amido hydrogens. A similar hydrogen bond pattern was previously observed for 9-deazapurine analogs (Ealick et al., 1991).

Although structural data for PNP complexes fail to favor the deprotonated purine base over the N7(H) tautomer, several features of the catalytic mechanism suggest that purine base deprotonation is more likely. Possibly the strongest argument for deprotonation is one based on the premise that enzymes that catalyze reversible reactions stabilize the same transition state in the forward and reverse directions. Since the phosphorolysis reaction does not involve N7-protonation of the purine nucleoside, nucleoside synthesis via the N7(H) tautomer would therefore entail a TS distinct from the TS used in phosphorolysis. If this were the case, then the TS in the phosphorolytic direction would utilize a negatively charged purine, whereas the TS in the synthesis direction would involve a positively charged purine nucleoside. The ability of an active site to accommodate two oppositely charged TSs is unlikely, unprecedented and counterintuitive to the notion that active sites stabilize polarized TSs in part through complementary electrostatic interactions.

A variety of experimental findings also support the use of the deprotonated purine base by PNP. For example, the guanine anion was postulated to be the species present in the PNP complex based on fluorescence changes (Porter, 1992). Furthermore, deprotonation of purines is consistent with the pK_a of purine bases, especially the pK_a of purine bases bound to proteins through complementary electrostatic interactions. In solution, the first pK_a of 6-oxopurines (e.g., hypoxanthine) is ∼9 and corresponds to deprotonation of N1 (Saenger, 1984). Since the pK_a of glutamate residues is <5, deprotonation of N1 by Glu201 is unlikely. Assuming that N1 is in the protonated form, N9 deprotonation appears

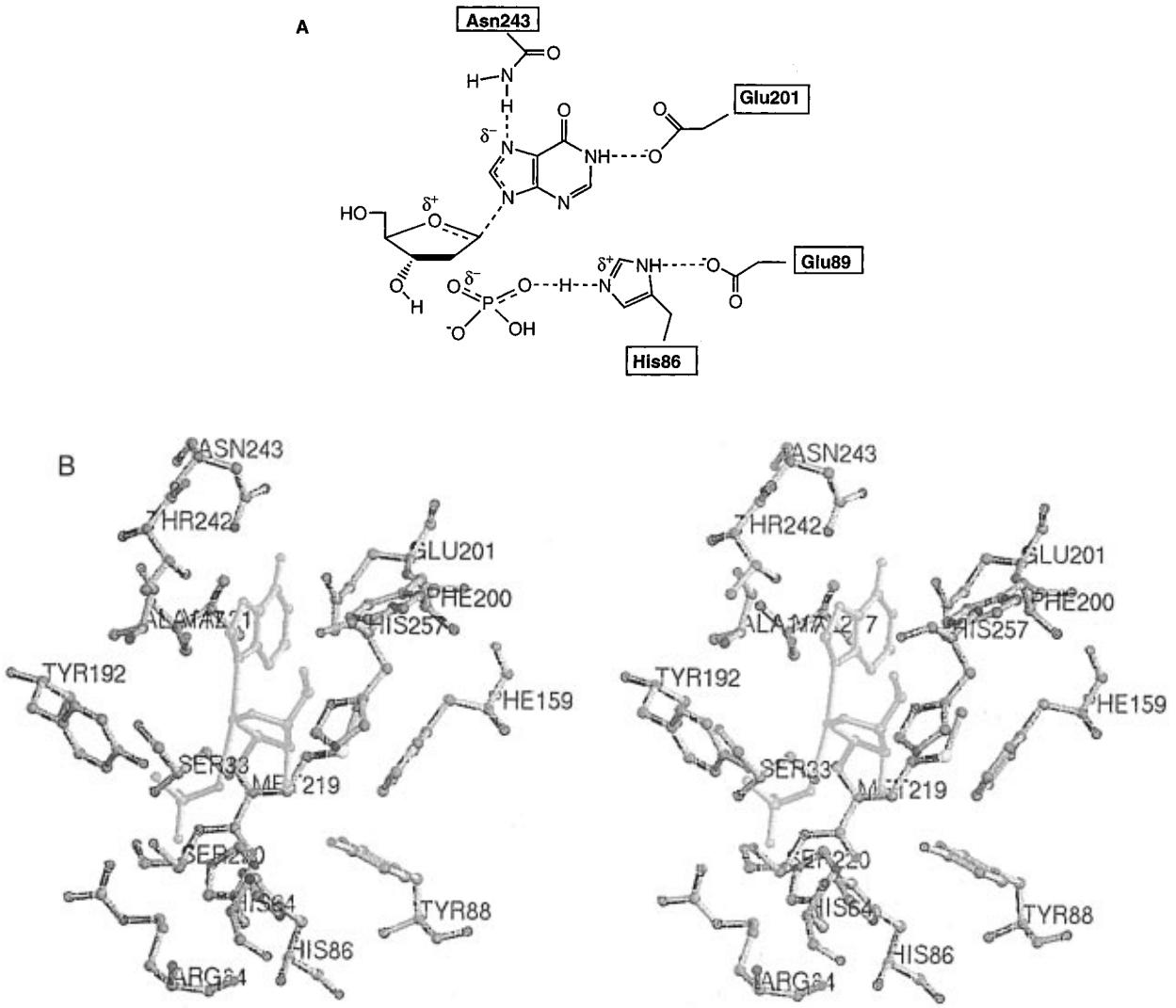

FIGURE 7: (A) Hypothetical model of the transition state structure stabilized by purine nucleoside phosphorylase. (B) Stereodrawing of the model prepared by averaging the atomic positions of structures resembling the reactant (purine nucleoside/phosphate) ternary complexes and structures resembling product (purine base/ribose 1-phosphate) ternary complexes. All amino acid residues with an atom within 4.0 Å of a substrate atom are included.

possible at physiological pH based on the pK_a of 1-methylguanine (pK_a = 10.5; Pfleiderer, 1961) and the likelihood that the pK_a of the E·S complex is even lower due to the hydrogen bond formed between Asn243 and N7. In addition to pK_a arguments, purine base deprotonation is supported by the observation that the Asn243Ala mutant exhibited an 80-fold increase in the K_M for hypoxanthine. This large increase in K_M for the base, but not the nucleoside, with the Asn243Ala mutant may signify that the base forms a stronger bond with Asn243 than the nucleoside. Purine base deprotonation is therefore consistent with this result, since a stronger hydrogen bond is expected to be formed between Asn243 and purines with a negatively charged N7 relative to purines with an uncharged N7.

Two findings that appear inconsistent with a single TS are the PNP-catalyzed synthesis of allopurinol riboside (7-deaza-8-azainosine) and 7-methylguanosine. Allopurinol riboside lacks N7 and therefore as expected is resistant to phosphorolysis. In the synthesis direction, allopurinol is a substrate for PNP generating allopurinol riboside in an irreversible manner (Krenitsky et al., 1967). Since nucleoside synthesis is proposed to involve N9-deprotonation and stabilization of the resulting monoanion by Asn243, allopurinol must follow a different mechanism. Possibly the 9-fold increase in K_M and the 35-fold decrease in k_{cat} relative to hypoxanthine results from the missing Asn243 interaction and its effect on the pK_a. If this were the only explanation, wild-type PNP and the Asn243Ala mutant would be expected to utilize allopurinol with equal efficiency. In fact, the Asn243Ala mutant showed an approximate 1000-fold decrease in k_{cat}/K_M for allopurinol riboside synthesis relative to wild-type (Table 2).

PNP-catalyzed synthesis of 7-methylguanosine from 7-methylguanine indicated that deprotonation is not always a necessary step in catalysis and that the neutral N9 of 7-methylguanine is sufficiently nucleophilic to react with ribose 1-phosphate. It therefore seemed possible that the N7(H) tautomer of purine bases could preferentially bind to PNP, using the hydrogen bond pattern identified previously for complexes of PNP with 9-deazaguanine analogs (Ealick et al., 1991), and react with ribose 1-phosphate in an analogous fashion to that of 7-methylguanine. Reaction of the N7(H) tautomer with ribose 1-phosphate would generate a positively charged nucleoside, which would subsequently undergo rapid deprotonation at physiological pH based on its pK_a (ca. 2).

Role of Ribose Binding Sites in Catalysis. Crystallographic studies indicated that the ribose binding pocket makes few contacts with the ligand relative to the purine or phosphate binding sites. In general, the β-face of the ribose is in contact with hydrophobic residues (Met219 near C2′ and Phe159 near C5′) whereas the α-face resides above the negatively charged phosphate and the highly polar phosphate binding site. Two residues within the ribose binding site are in hydrogen bond contact with the nucleoside, namely His257 and Tyr88, which form hydrogen bonds to the 5′- and 3′-hydroxyls, respectively. The O3′-hydroxyl is also in hydrogen bond contact with one of the phosphate oxygens. These residues along with Met219 and Phe159 are strictly conserved among the eight other nucleoside phosphorylases with known sequences and specificity for 6-oxopurine nucleosides (Figure 6).

His257 has been postulated (Kline & Schramm, 1993) to play a role in catalysis based on its hydrogen bond to O5′ and reports that 5′-deoxyinosine is resistant to phosphorolysis (Jordon & Wu, 1978). Kinetic isotope studies on the calf spleen PNP as well as ab initio calculations on a TS model suggested that the hydrogen bond between His257 and the 5′-hydroxyl is a prominent feature of the TS (Kline & Schramm, 1995). In contrast, our studies suggest that His257 plays a relatively minor role in the catalytic mechanism and in TS stabilization based on the finding that the His257Ala mutant exhibits similar kinetics to wild-type PNP (Erion et al., 1997). Consistent with this conclusion were kinetic results, which in contrast to the results of Jordan and Wu (1978), showed 5′-deoxyinosine to be an excellent substrate for PNP (Stoeckler et al., 1980).

Role of Phosphate Binding Sites in Catalysis. Crystallographic analyses of nucleoside analogs bound to PNP showed the phosphate to hydrogen bond with at least four active-site residues as well as with the C3′-hydroxyl of the ribose. The X-ray structures also showed the phosphate to reside on the α-face of the ribose with one oxygen within 3.3 Å of the ribose C1′ and in good alignment for backside displacement of the purine base. The relative location of phosphate to nucleoside accounts for the high stereospecificity of the PNP reaction and supports a mechanism in which the C1′ of ribose undergoes nucleophilic attack by phosphate. Kinetic isotope studies further suggested that the phosphorolysis reaction proceeds by an S_N1-type mechanism and an oxocarbenium ion intermediate. To date all other enzymes that cleave a glycosidic bond (e.g., glycosidases such as lysozyme) follow an S_N1-type mechanism. In addition, each enzyme is thought to stabilize the intermediate oxocarbenium ion with an anionic active-site residue (Kirby, 1987). Since anionic residues were not observed near the ribosyl oxygen in X-ray structures of PNP complexes, it was concluded that phosphorylases catalyze glycosidic bond cleavage by a mechanism distinct from glycosidases.

One mechanism that is consistent with the PNP crystal structure employs the phosphate as the anionic residue that stabilizes the intermediate oxocarbenium ion. Participation of phosphate in the TS (Figure 7) can be inferred from several experimental findings and theoretical arguments. The importance of phosphate in glycosidic bond cleavage is apparent from the poor hydrolytic activity of PNP (Kim et al., 1968) which is at least 4 orders of magnitude slower than either nucleoside phosphorolysis or arsenolysis (Kline & Schramm, 1993). A recent study of PNP-catalyzed hydrolysis, methanolysis, and arsenolysis of inosine supported a transition state with oxocarbenium character and little participation by the attacking solvent molecule (Kline & Schramm, 1995). Thus, in the absence of phosphate, glycosidic bond cleavage proceeds very slowly with the oxocarbenium ion intermediate rapidly trapped by the solvent molecules (water or methanol) that occupy the empty phosphate binding site (Kline & Schramm, 1995). Participation of phosphate in the transition state is also consistent with the pH-rate profile reported for PNP-catalyzed nucleoside phosphorolysis and arsenolysis (Jordon & Wu, 1978). The apparent pK_a values on the acid side of the pH rate profile were 6.1 and 5.3 for the phosphorolysis and arsenolysis reactions, respectively. These results suggested that the titratable species in the E·S complex was the inorganic phosphate, since the apparent pK_as were well within the range of the second pK_a of phosphate (7.2) and arsenate (6.8) and in the same rank order. Since the rate-determining step in the phosphorolysis reaction is glycosidic bond cleavage and not nucleophile addition to the oxocarbenium ion intermediate, these results suggest that phosphate aids glycosidic bond cleavage presumably through stabilization of the TS in addition to acting as the nucleophile in the reaction. Less clear is the ionic state of the catalytically active phosphate, although the results of Jordon and Wu (1978) appear to favor the dianion over the trianion.

Participation of the phosphate dianion in the reaction could arise either from preferential binding of the dianion to the phosphate binding site or by deprotonation of the monoanion by an active-site base. The two possibilities are difficult to differentiate by structure or kinetics. The phosphate binding site can accommodate either the mono- or dianion with one negatively charged oxygen near Arg84 and the other oxygens participating in multiple hydrogen bonds to the protein. One of the contacts is to the imidazole of His86, which could serve either as an active-site base or as a residue that helps preferentially bind the dianion by existing as the positively charged imidazolium ion. Some previously reported results seem to support a role of His86 in the catalytic mechanism. For example, chemical modification studies using the dye-sensitized photooxidation method for modification of histidines produced an enzyme with a substantially higher apparent pK_a (Jordan & Wu, 1978; Lewis & Glantz, 1976). The mutant His86Ala, however, exhibited only minor effects on catalytic efficiency at pH 7, suggesting that in the absence of the His86 imidazole, the dianion can still bind and participate in phosphorolysis (Erion et al., 1997).

Further analysis of the phosphate binding site showed that the imidazole of His86 is hydrogen bonded not only to the phosphate but also to the side-chain carboxyl of Glu89. The interaction with Glu89 is reminiscent of the catalytic triad found in serine proteases (Blow et al., 1969) and the catalytic diad found in PLA_2 (Li & Tsai, 1993). In these examples, the carboxylate is used either to orientate the imidazole so that the basic lone pairs on the nitrogen are available for deprotonation of the nucleophile or to increase the basicity of the imidazole through stabilization of the resulting positively charged imidazolium ion. In contrast to the His−Asp(Glu) diads found in serine and cysteine proteases, the His/Glu pair of PNP resides close in sequence and at the first and last positions of a β-turn. This arrangement locks the His/Glu pair into a rigid conformation with the imidazole of His86 in direct contact with the phosphate. Although the

presence of this structural motif and the finding that both His86 and Glu89 are strictly conserved across nucleoside phosphorylases (Figure 6) provide some support for the potential importance of these residues in catalysis, alanine mutants of His86 and Glu89 may suggest otherwise given the relatively modest effect of these mutations on activity (Erion et al., 1997). Kinetic results obtained using the Glu89Ala mutant showed a 23-fold loss in the K_M for phosphate but little change in k_{cat} for either phosphorolysis or nucleoside synthesis. Interestingly, the Glu89Lys mutant isolated from PNP deficient children is reported to have no catalytic activity (Williams et al., 1987). The difference in activity between the mutants may arise from placing a positively charged Lys in a region that electrostatically accommodates a negatively charged Glu. On the other hand, the ability of PNP to catalyze the phosphorolysis of nucleosides in the absence of His86 is consistent with the relatively low second pK_a (~7) of phosphate and, therefore, the presence of the dianion at physiological pH.

Since both the phosphate mono- and dianion species are available to PNP, it is interesting to speculate why PNP uses the dianion for catalysis. One possibility is that the dianion is more nucleophilic than the monoanion. The importance of phosphate nucleophilicity is unclear, however, since the monoanion is still a good nucleophile and therefore should trap the oxocarbenium ion intermediate without compromising the catalytic rate (rate-determining step is glycosyl bond cleavage). An alternative explanation that could account for the importance of the dianion on catalytic rate is the participation of the dianion in the TS. In this case, the phosphate binds as the monoanion with one of its oxygens near both the ribosyl endocyclic oxygen and C1′. Deprotonation by His86 increases the negative charge on the phosphate oxygen which in turn polarizes the glycosidic bond through electrostatic strain. As the glycosidic bond breaks, the resulting oxocarbenium ion is stabilized by the negatively charged phosphate.

These results are reminiscent of other mechanistic studies showing that preassociation of nucleophiles with carbenium ions generated during an S_N1 bond cleavage reaction aids in the formation and stabilization of the TS (Jenks, 1980). Similar to PNP, glycogen phosphorylase b has been postulated to use phosphate to stabilize an intermediate oxocarbenium ion (Johnson et al., 1990). Unlike PNP, however, glycogen phosphorylase is postulated to initiate glycosidic bond cleavage by using the bound phosphate for protonation of the glycosidic oxygen, which in turn promotes cleavage of the glycosidic bond and production of the oxocarbenium ion intermediate.

Purine Nucleoside Binding Conformation. Crystallographic analyses of PNP complexes indicated that purine nucleosides bind with the purine base aligned along the C1′−C2′ bond of the ribose (Figure 6). The average dihederal angle as defined by O4′−C1′−N9−C4 was 145°, which by the Klyne and Prelog convention classifies the glycosidic bond as +*anticlinal* (+*ac*). This torsion angle is unusual considering the range of torsion angles determined for purine nucleosides in the crystalline state by X-ray analysis, in solution by NMR analysis (via coupling constants and/or NOEs), and in other macromolecular complexes (proteins and oligonucleotides) by a variety of techniques (Sundaralingam, 1969; Saenger, 1983b). For comparison, the most common torsions for nucleosides exhibiting a C3′-*endo* sugar pucker range from −60° to −90° (high *anti*). Evidence for the +*anticlinal* conformation may also be reflected in the sugar pucker, which was readily assigned as C4′-*endo*, despite the modest resolution (2.7−3.2 Å), based on the consistency of the electron density found for the sugar for a wide variety of nucleoside analogs. A similar binding conformation was also found for nucleosides bound to bovine PNP, which was solved recently at significantly higher resolution (1.8 Å; Mao, C., & Ealick, S. E., unpublished results). Analysis of the active-site structure revealed the residue contacts that confine the nucleoside to the observed +*ac* conformation. Movement of the purine base is restricted by hydrogen bonds to N1 and possibly O6 and N7 and by hydrophobic interactions involving the side chains of Phe200 and Ala116 to both faces of the purine ring. The ribose is confined to a single region of the active site by hydrogen bonds between O3′ and both Tyr88 and the phosphate as well as by a hydrophobic contact with Met219 and possibly Phe159 to the ribose β-face. Interestingly, Met219 is conserved in all nucleoside phosphorylases regardless of base specificity.

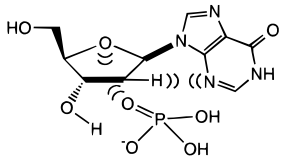

FIGURE 8: Ligand strain in the ternary complex.

The consistent finding of a relatively uncommon glycosidic bond torsion angle for nucleosides bound to PNP suggested that the binding conformation may play an important role in phosphorolysis (Figure 8). The difference in energy between the nucleoside conformation observed in the PNP active site and the standard high *anti* conformation found in solution was calculated to be just over 3 kcal/mol using geometry optimized structures and the Hartree−Folk molecular orbital method at the 6-31G** level. Since the energy difference is derived from gas phase calculations, the magnitude of the difference serves only as a qualitative measure of the potential ligand strain associated with nucleosides complexed to PNP. Nevertheless, it is clear that the conformational energy difference must be considerable and therefore that phosphorolysis could be accelerated through steric strain relief.

In addition to steric strain, the +*ac* conformation may also enhance phosphorolysis through "electrostatic strain" (Warshel & Levitt, 1976; Cherian et al., 1990). Restricting the glycosidic bond to the +*ac* conformation places the endocyclic ribosyl oxygen directly above the negatively charged phosphate oxygen. The close proximity of both oxygens would be expected to produce lone pair repulsion and correspondingly some electrostatic strain in the ternary complex (Figure 8). In contrast, the TS is stabilized through an attractive electrostatic interaction between the oxocarbenium ion and the negatively charged phosphate. Deprotonation of the phosphate in the ternary complex increases the negative charge on the phosphate and thereby further diminishes the energy difference between the ground state and TS. Accordingly, phosphorolysis is accelerated by relieving the electrostatic strain through weakening of the glycosidic bond and formation of the oxocarbenium ion.

Summary of Catalytic Mechanism. Structural data generated from X-ray crystallography and molecular modeling

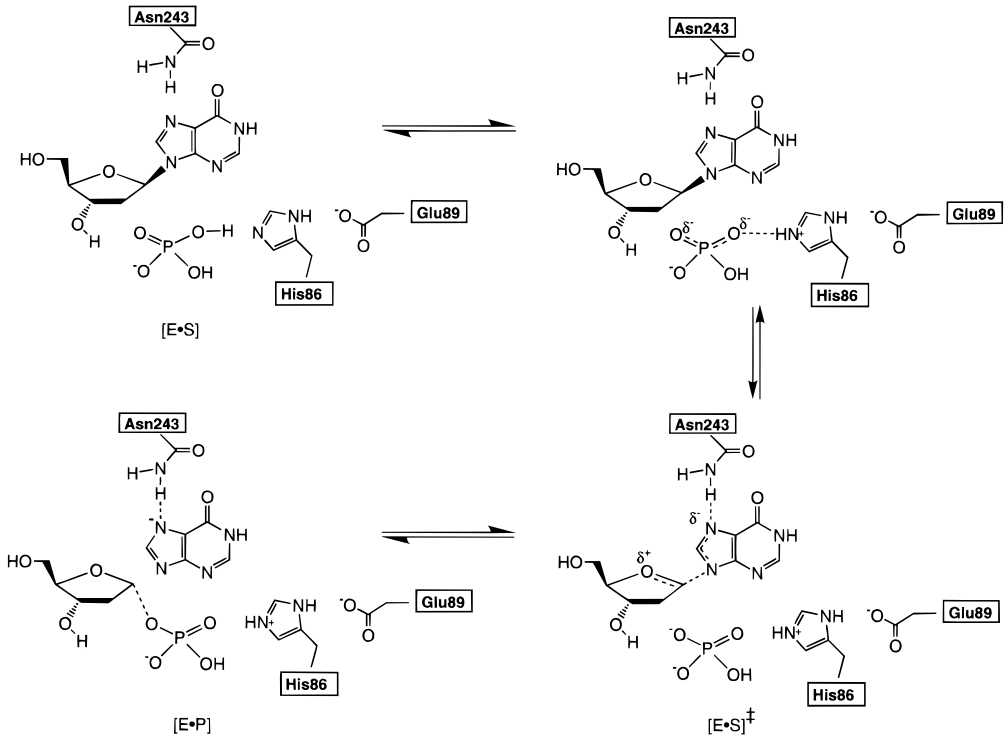

FIGURE 9: Proposed PNP catalytic mechanism.

studies and enzyme kinetic data generated using PNP mutants and a variety of pseudosubstrate analogs suggest that PNP catalyzes the reversible phosphorolysis of purine nucleosides using the substrate-assisted catalytic mechanism shown in Figure 9. Efficient catalysis is achieved by formation of a high-energy ground state complex and by using active-site residues and the cosubstrate phosphate to stabilize the TS.

In the phosphorolytic direction, glycosidic bond cleavage is facilitated by binding a high-energy nucleoside conformation (+*ac*) and by invoking electrostatic strain in the ground state complex. Electrostatic strain develops during the deprotonation of the phosphate monoanion to the dianion by His86. The resulting positively charged histidine is stabilized by Glu89 through a charge-transfer relay system reminiscent of the catalytic triad found in serine proteases and other enzymes. Phosphate deprotonation increases its nucleophilicity and places greater negative charge in the vicinity of the endocyclic ribosyl oxygen. As negative charge on the phosphate oxygen increases, electron repulsion between the negatively charged phosphate oxygen and electron pairs on the endocyclic ribosyl oxygen leads to electrostatic strain and weakening of the glycosidic bond. As glycosidic bond breakage proceeds, an intermediate oxocarbenium ion is formed and simultaneously stabilized by the phosphate dianion. Thus, the proposed substrate-assisted catalytic mechanism utilizes phosphate to both initiate bond cleavage and to stabilize the intermediate oxocarbenium ion through formation of a tight ion pair. Use of phosphate for stabilization of the intermediate oxocarbenium ion is the key structural feature that differentiates phosphorylases from glycosidases (e.g., lysozyme) and nucleosidases (e.g., AMP nucleosidase).

Glycosidic bond cleavage results in an accumulation of electron density on the purine ring. Delocalization of the negative charge onto N9 and N7 is predicted from quantum mechanical calculations of three possible guanine tautomers (Scheme 2). In the proposed catalytic mechanism, the resulting negatively charged purine base is stabilized by a hydrogen bond formed between Asn243 and N7. This hydrogen bond preferentially stabilizes the TS relative to the ground state due to the greater hydrogen bond strength inherent to hydrogen bonds involving charged groups. Hence, glycosidic bond cleavage proceeds through a TS that entails a "push-pull" type effect in which ionization of phosphate pushes electrons from the endocyclic ribosyl oxygen into the C1′−O bond, thereby weakening the glycosidic bond, while at the same time the Asn243−N7 hydrogen bond pulls electrons from the glycosidic bond onto the purine ring. After cleavage of glycosidic bond, ribose 1-phosphate dissociates from the active site and the negatively charged purine is reprotonated by water. The final step is release of the neutral purine base.

In the synthesis direction, the catalytic mechanism is expected to be the reverse of the steps outlined for nucleoside phosphorolysis. Furthermore, since the reaction catalyzed by PNP is reversible, the TS stabilized by PNP is postulated to be identical for both nucleoside synthesis and nucleoside phosphorolysis. Hence, nucleoside synthesis results after Asn243-assisted purine base deprotonation and solvolysis of ribose 1-phosphate to form an intermediate, phosphate-stabilized, oxocarbenium ion. Cleavage of the phosphate is enhanced by the residues in contact with the phosphate. Trapping of the oxocarbenium ion by the purine base completes the reaction.

ACKNOWLEDGMENT

We thank Ms. Rose Marie Smith and Shih-Ying Li for technical assistance in the evaluation of substrate analogs, Dr. Ken Takabayashi for providing the sequences to the rat and *Bacillus stearothermophilus* PNPs, and Ms. Lisa Weston for her assistance in preparing this manuscript. We also thank the editor (P. A. Frey) for his comments on the mechanism involving the enol tautomer (footnote 5).

REFERENCES

Agarwal, R. P., & Parks, R. E., Jr. (1971) *J. Biol. Chem. 246*, 3763−3768.

Blake, C. C. F., Mair, G. A., North, A. C. T., Phillips, D. C., & Sarma, V. R. (1967) *Proc. R. Soc. London, Ser. B 167*, 365.

Blow, D. M., Birktoft, J. J., & Hartley, B. S. (1969) *Nature 221*, 337.

Brünger, A. T. (1992) *X-PLOR. Version 3.1. A System for X-ray Crystallography and NMR*; Yale University Press, New Haven, CN.

Bzowska, A., Kulikowska, E., & Shugar, D. (1990) *Z. Naturforsh. 45*, 59−70.

Bzowska, A., Luic, M., Schroder, W., Shugar, D., Saenger, W., & Koellner, G. (1995) *FEBS Lett. 367*, 214−218.

Carlson, J. D., & Fischer, A. G. (1979) *Biochim. Biophys. Acta 571*, 21−34.

Carson, M., & Bugg, C. E. (1986) *J. Mol. Graphics 4*, 121−122.

Cherian, X. M., Van Arman, S. A., & Czarnik, A. W. (1990) *J. Am. Chem. Soc. 112*, 4490−4498.

Cook, W. J., Ealick, S. E., Bugg, C. E., Stoeckler, J. D., & Parks, R. E., Jr. (1981) *J. Biol. Chem. 256*, 4079−4080.

Dreyfus, M., Dodin, G., Bensaude, O., & Dubois, J. E. (1975) *J. Am. Chem. Soc. 97*, 2369−2376.

Ealick, S. E., Rule, S. A., Carter, D. C., Greenhough, T. J., Babu, Y. S., Cook, W. J., Habash, J., Helliwell, J. R., Stoeckler, J. D., Parks, R. E., Jr., Chen, S. F., & Bugg, C. E. (1990) *J. Biol. Chem. 243*, 1812−1820.

Ealick, S. E., Babu, Y. S., Bugg, C. E., Erion, M. D., Guida, W. C., Montgomery, J. A., & Secrist, J. A., III (1991) *Proc. Natl. Acad. Sci. U.S.A. 88*, 11540−11544.

Erion, M. D., Niwas, S., Rose, J. D., Ananthan, S., Allen, M., Secrist, J. A. III, Babu, Y. S., Bugg, C. E., Guida, W. C., Ealick, S. E., Montgomery, J. A. (1993) *J. Med. Chem. 36*, 3771−3783.

Erion, M. D., Takabayashi, K., Smith, H. B., Kessi, J., Wagner, S., Honig, S., Shames, S. L., & Ealick, S. E. (1997) *Biochemistry 36*, 11725−11734.

Fersht, A. R., Shi, J.-P., Knill-Jones, J., Lowe, D. M., Wilkinson, A. J., Blow, D. M., Brick, P., Carter, P., Waye, M. M. Y., & Winter, G. (1985) *Nature 314*, 235−238.

Frisch, M. J., Trincks, G. W., Schlegel, H. B., Gill, P. M. W., Johnson, B. G., Wong, M. W., Foresman, J. B., Robb, M. A., Head-Gordon, M., Replogle, E. S., Gomparts, R., Andres, J. L., Raghavachar, K., Brinkley, J. S., Gonzalaz, C., Morton, R. L., Fox, D. J., DeFrees, D. J., Baker, J., Stewart, J. J. P., & Pople, J. A. (1993) Gaussian Inc., Pittsburgh, PA.

Garrett, E. R., & Mehta, P. J. (1972) *J. Am. Chem. Soc. 94*, 8532−8541.

Horenstein, B. A., Parkin, D. W., Estupinan, B., & Schramm, V. L. (1991) *Biochemistry 30*, 10788−10795.

Howard, A. J., Gilliland, G. L., Finzel, B. C., Poulos, T. L., Ohlendorf, D. H., & Salemme, F. R. (1987) *J. Appl. Crystallogr. 20*, 383−387.

Izatt, R. M., Christensen, J. J., & Rytting, H. J. (1971) *Chem. Rev. 71*, 439−453.

Jenks, W. P. (1980) *Acc. Chem. Res. 13*, 161−169.

Jenuth, J. P., & Snyder, F. F. (1991) *Nucleic Acids Res. 19*, 1708.

Johnson, L. N., Acharya, K. R., Jordan, M. D., & McLaughlin, P. J. (1990) *J. Mol. Biol. 211*, 645−661.

Jordan, F., & Wu, A. (1978) *J. Med. Chem. 21*, 877−882.

Kim, B. K., Cha, S., & Parks, R. E., Jr. (1968) *J. Biol. Chem. 243*, 1771−1776.

Kirby, A. J. (1987) *CRC Crit. Rev. Biochem. 22*, 283−315.

Kline, P. C., & Schramm, V. L. (1993) *Biochemistry 32*, 13212−13219.

Kline, P. C., & Schramm, V. L. (1995) *Biochemistry 34*, 1153−1162.

Kline, P. C., & Schramm, V. L. (1992) *Biochemistry 31*, 5964−5973.

Krenitsky, T. (1967) *Mol. Pharmacol. 3*, 526−536.

Krenitsky, T., Elion, G. B., Strelitz, R. A., & Hitchings, G. H. (1967) *J. Biol. Chem. 242*, 2675.

Krenitsky, T., Elion, G. B., Henderson, A. M., & Hitchings, G. H. (1968) *J. Biol. Chem. 243*, 2876.

Kulikowska, E., Bzowska, A., Wierchowski, J., & Shugar, D. (1986) *Biochim. Biophys. Acta 874*, 355−363.

Lehikoinen, P. K., Sinnott, M. L., & Krenitsky, T. A. (1989) *Biochem. J. 257*, 355−359.

Lewis, A. S., & Glantz, M. D. (1976) *Biochemistry 15*, 4451−4456.

Lewis, A. S., & Lowy, B. A. (1979) *J. Biol. Chem. 254*, 9927−9932.

Li, Y., & Tsai, M.-D. (1993) *J. Am. Chem. Soc. 115*, 8523−8526.

Lonnberg, H., & Lehikoinen, P. (1982) *Nucleic Acids Res. 10*, 4339−4349.

Mohamadi, F., Richards, N. G. J., Guida, W. C., Liskamp, R., Caufield, C., Chang, G., Hendrickson, T., & Still, W. C. (1990) *J. Comput. Chem. 11*, 440.

Montgomery, J. A., Niwas, S., Rose, J. D., Secrist, J. A., III, Babu, Y. S., Bugg, C. E., Erion, M. D., Guida, W. C., Ealick, S. E. (1993) *J. Med. Chem. 36*, 55−69.

Parkin, D. W., Mentch, F., Banks, G. A., Horenstein, B. A., & Schramm, V. L. (1991) *Biochemistry 30*, 4586−4594.

Parks, R. E., Jr., & Agarwal, R. P. (1972) *Enzymes*, 3rd ed.; vol 7, pp 483−514.

Pfleiderer, W. (1961) *Justus Liebigs Ann. Chem. 647*, 167.

Porter, D. J. T. (1992) *J. Biol. Chem. 267*, 7342−7351.

Romero, R., Stein, R., Bull, H. G., & Cordes, E. H. (1978) *J. Am. Chem. Soc. 100*, 7620−7624.

Ropp, P. A., & Traut, T. W. (1991) *J. Biol. Chem. 266*, 7682−7687.

Sack, J. (1988) *J. Mol. Graphics 6*, 224.

Saenger, W. (1984a) in *Principles of Nucleic Acid Structure* (Cantor, C. R., Ed.) pp 51−104 Springer-Verlag, New York.

Saenger, W. (1984b) in *Principles of Nucleic Acid Structure* (Cantor, C. R., Ed.) pp 107−110 Springer-Verlag, New York.

Salamone, S. J., & Jordan, F. (1982) *Biochemistry 21*, 6382−6388.

Seeger, C., Poulsen, C., & Dandanell, G. (1995) *J. Bacteriol. 177*, 5506−5516.

Stein, R. L., & Cordes, E. H. (1981) *J. Biol. Chem*. 256, 767−772.

Stoeckler, J. D. (1984) in *Developments in Cancer Chemotherapy* (Glazer, R. I., Ed.) pp 35−60.

Stoeckler, J. D., Cambor, C., & Parks, R. E., Jr. (1980) *Biochemistry 19*, 102−107.

Stoeckler, J. D., Poirot, A. F., Smith, R. M., Parks, R. E., Jr., Ealick, S. E., Takabayashi, K., & Erion, M. D. (1997) *Biochemistry 36*, 11749−11756.

Sundaralingam, M. (1969) *Biopolymers 7*, 821−860.

Walter, R. L., Symersky, J., Poirot, A. F., Stoeckler, J. D., Erion, M. D., & Ealick, S. E. (1994) *Nucleosides Nucleotides 13*, 689−706.

Warshel, A., & Levitt, M. (1976) *J. Mol. Biol. 103*, 227.

Wells, J. A. Cunningham,B. C., Graycar, T. P., & Estell, D. A. (1986) *Philos. Trans. R. Soc. London A, 317*, 415.

Williams, S. R., Goddard, J. M., & Martin, D. W., Jr. (1984) *Nucleic Acid Res. 12*, 5779−5787.

Williams, S. R., Gekeler, V., McIvor, R. S., & Martin, D. W., Jr. (1987) *J. Biol. Chem. 262*, 2332−2338.

Zimmerman, T. P., Gersten, N. B., Ross, A. F., & Miech, R. P. (1971) *Can. J. Biochem. 49*, 1050−1054.

Zoltewicz, J. A., Clark, D. F., Sharpless, T. W., & Grahe, G. (1970) *J. Am. Chem. Soc. 92*, 1741−1749.

BI961970V